doi:10.1016/j.jmb.2010.08.007 J. Mol. Biol. (2010) 402, 560–577

Contents lists available at www.sciencedirect.com

Journal of Molecular Biology

journal homepage: http://ees.elsevier.com.jmb

Structure of the AML1-ETO NHR3–PKA(RIIα) Complex and Its Contribution to AML1-ETO Activity

Takeshi Corpora[1], Liya Roudaia[2], Zaw Min Oo[3], Wei Chen[2], Ekaterina Manuylova[2], Xiongwei Cai[3], Michael J. Chen[3], Tomasz Cierpicki[4], Nancy A. Speck[3]* and John H. Bushweller[1,4]*

[1]*Department of Chemistry, University of Virginia, Charlottesville, VA 22906, USA*
[2]*Department of Biochemistry, Dartmouth Medical School, Hanover, NH 03755, USA*
[3]*Abramson Family Cancer Research Institute and Department of Cell and Developmental Biology, University of Pennsylvania, Philadelphia, PA 19103, USA*
[4]*Department of Molecular Physiology and Biological Physics, University of Virginia, Charlottesville, VA 22908, USA*

Received 5 July 2010;
accepted 4 August 2010
Available online
11 August 2010

Edited by M. F. Summers

Keywords:
AML1-ETO;
leukemia;
AKAP;
PKA(RIIα);
NHR3

AML1-ETO is the chimeric protein product of t(8;21) in acute myeloid leukemia. The ETO portion of the fusion protein includes the nervy homology region (NHR) 3 domain, which shares homology with A-kinase anchoring proteins and interacts with the regulatory subunit of type II cAMP-dependent protein kinase A (PKA(RIIα)). We determined the solution structure of a complex between the AML1-ETO NHR3 domain and PKA(RIIα). Based on this structure, a key residue in AML1-ETO for PKA(RIIα) association was mutated. This mutation did not disrupt AML1-ETO's ability to enhance the clonogenic capacity of primary mouse bone marrow cells or its ability to repress proliferation or granulocyte differentiation. Introduction of the mutation into AML1-ETO had minimal impact on *in vivo* leukemogenesis. Therefore, the NHR3–PKA(RIIα) protein interaction does not appear to significantly contribute to AML1-ETO's ability to induce leukemia.

© 2010 Elsevier Ltd. All rights reserved.

Introduction

AML1-ETO is a chimeric protein that is commonly observed in acute myeloid leukemia (AML) of the M2 subtype.[1] This aberrant protein results from t(8;21), which fuses the N-terminus of AML1 (encoded by *RUNX1*) with most of ETO (*e*ight *t*wenty *o*ne, encoded by *RUNXT1*). AML1-ETO contains five highly conserved domains: the DNA and core binding factor (CBF) β binding region of AML1 (known as the Runt domain) and nervy homology regions (NHRs) 1–4 from ETO.[2–4]

Multiple studies have examined the contribution of these five conserved domains to AML1-ETO's activities following retroviral transduction into primary bone marrow (BM) cells. These studies have assessed a variety of AML1-ETO's activities, including its abilities to inhibit proliferation in *ex vivo* BM cultures, to impair granulocyte

*Corresponding authors. J. H. Bushweller is to be contacted at Department of Molecular Physiology and Biological Physics, University of Virginia, UVa Health Sciences Center, PO Box 800736, Charlottesville, VA 22908, USA. E-mail addresses: nancyas@exchange.upenn.edu; jhb4v@virginia.edu.

Present address: T. Cierpicki, Department of Pathology, University of Michigan, Ann Arbor, MI 48109, USA.

Abbreviations used: NHR, nervy homology region; PKA(RIIα), regulatory subunit of type II cAMP-dependent protein kinase A; AML, acute myeloid leukemia; CBF, core binding factor; BM, bone marrow; AKAP, A-kinase anchoring protein; PKA, protein kinase A; ITC, isothermal titration calorimetry; Trx, thioredoxin; NOE, nuclear Overhauser enhancement; RDC, residual dipolar coupling; PKA(RIα), regulatory subunit of type I cAMP-dependent protein kinase A; GFP, green fluorescent protein; SCF, stem cell factor; RISR, RI specifier region; EDTA, ethylenediaminetetraacetic acid.

differentiation, to confer enhanced serial replating, and to cause leukemia in conjunction with secondary mutations. DNA binding and CBFβ binding by the Runt domain were demonstrated to be essential for all of these aforementioned activities.[5–8] Deletions of NHR1 (also known as the TATA-box-binding protein association factor homology domain or eTAFH) or mutations that impaired the interaction of NHR1 with E proteins, on the other hand, did not severely affect AML1-ETO's activities.[6,8,9] The NHR2 domain, also known as the hydrophobic heptad repeat, is an α-helical tetramer that acts as the ETO oligomerization domain and is crucial for all of AML1-ETO's activities.[6,8,10,11] NHR3 is an amphipathic α-helical rod that interacts with the regulatory subunit of type II cAMP-dependent protein kinase A (PKA (RIIα)).[4] Deletion of NHR3 had no effect on AML1-ETO's ability to confer serial replating activity.[6] NHR4, or the MYND (*my*eloid *n*ervy *D*EAF-1) domain, is a member of the RING finger structural family that binds SMRT and N-CoR corepressors, as well as a putative RNA/DNA binding protein called SON.[12–16] A C-terminal truncation of AML1-ETO that removed both NHR3 and NHR4 domains actually conferred onto AML1-ETO the ability to cause leukemia in the absence of experimentally induced secondary mutations, indicating that one or both domains actually interfere with some of the leukemogenic functions of AML1-ETO.[17,18] Deletion of NHR4 alone, or the introduction of mutations that disrupt its three-dimensional structure, also augmented AML1-ETO's leukemogenic activity in mice.[16] The contribution of NHR3 alone to AML1-ETO's leukemogenic activity has not been assessed.

The NHR3 domain of AML1-ETO shares some sequence homology with A-kinase anchoring proteins (AKAPs), which act as scaffolding proteins that associate with cAMP-dependent protein kinase A (PKA).[4,19–21] AKAPs are believed to facilitate the compartmentalization of PKA for the phosphorylation of specific targets in intracellular signal transduction pathways and to incorporate cAMP signaling into different pathways and signaling events by dictating the formation of multiprotein complexes.[19,20,22] The compartmentalization of PKA determines when and where a phosphorylation event takes place, emphasizing the importance of AKAPs in signal transduction. PKA is a holoenzyme comprising two catalytic subunits (C) and a regulatory homodimer (RIIα).[19–21,23] Phosphorylation of target substrates is catalyzed by the C subunits, while localization of PKA is determined through the R subunit and its interaction with certain AKAPs.[21,24–26] Previous yeast-two-hybrid studies showed that AML1-ETO specifically interacts with PKA(RIIα) through the NHR3 domain, suggesting that the ETO domain acts as a novel AKAP.[4]

While the structure of PKA(RIIα), as well as the structures of several PKA(RIIα)–AKAP complexes, has been reported,[27,28] neither the structure of the AML1-ETO NHR3 domain nor the structure of its complex with PKA(RIIα) has been determined. In order to better understand the role of AML1-ETO–PKA(RIIα) interaction in leukemogenesis, we determined the structure of this protein–protein complex. Based on the structure, a mutation that decreased the binding of NHR3 to PKA(RIIα) by approximately 50-fold was identified. This mutation did not abolish AML1-ETO's ability to enhance the clonogenic capacity of primary mouse BM cells, nor did it ameliorate its acute block on proliferation or granulocyte differentiation. This 50-fold reduction in NHR3–PKA(RIIα) binding was also insufficient to impair AML1-ETO's ability to cause leukemia in cooperation with an activated tyrosine kinase (TEL-PDGFβR).

Results

Solution structure of the NHR3–PKA(RIIα) complex

Structural studies of the isolated NHR3 domain were complicated by the fact that much of the domain is unstructured. Circular dichroism (CD) spectroscopy showed that the NHR3 domain contains an approximately 25% α-helical secondary structure, with the remainder being random coil. This was confirmed with a ^{15}N–^{1}H heteronuclear single quantum coherence experiment that revealed a poorly dispersed spectrum (Supplementary Fig. 1a). However, when the NHR3 domain was titrated with PKA(RIIα), signal dispersion improved, indicating that the NHR3 domain forms a defined structure only upon complex formation with PKA (RIIα) (Supplementary Fig. 1a). Although there was observed improvement in the spectrum upon addition of PKA(RIIα), the quality of the NHR3 domain spectrum was not sufficient for assignment. Therefore, we used a combination of limited proteolysis and mass spectroscopy to identify portions of the NHR3 domain that are not structured in the NHR3–PKA(RIIα) complex. Based on these data, we produced a truncated construct of the NHR3 domain (A585-A615). While the spectrum of the NHR3(585–615) construct was still poorly dispersed, the spectrum of this construct in complex with PKA(RIIα) was very well dispersed and easily assignable (Supplementary Fig. 1b).

Isothermal titration calorimetry (ITC) data showed that the binding of wild-type NHR3 domain to the PKA(RIIα) dimer occurs with high affinity (K_d = 67 nM) and a stoichiometry of 1:2 (data not shown). To verify that truncation of the domain to

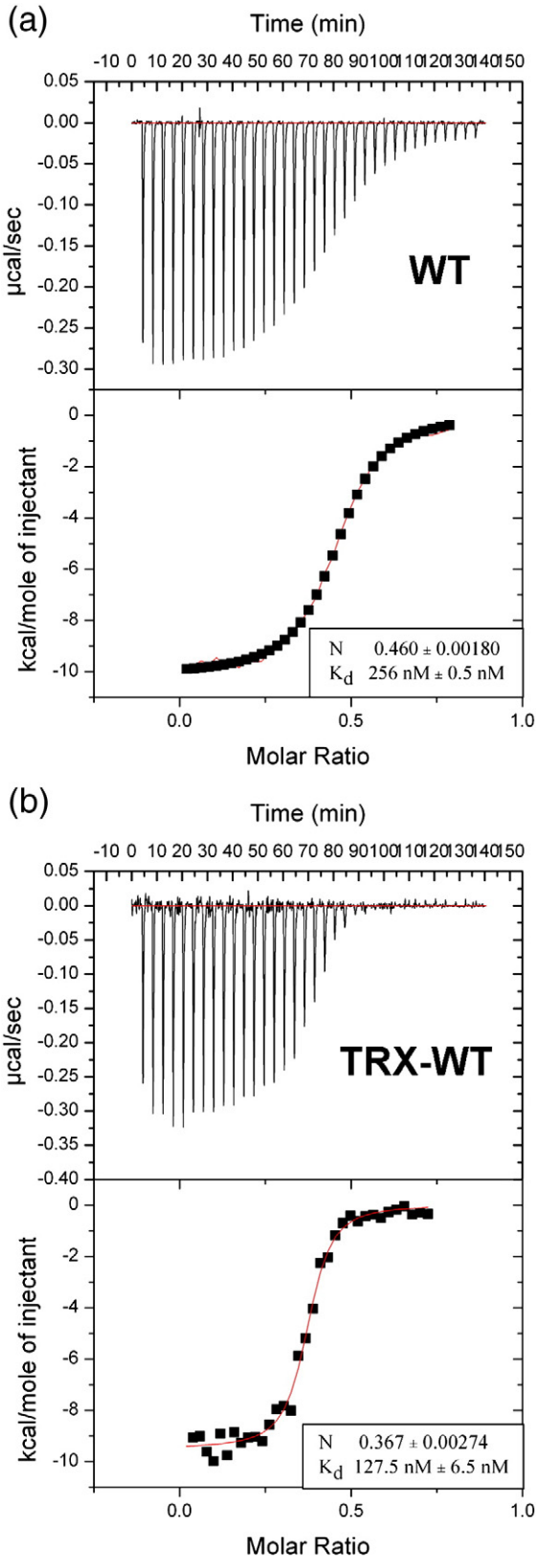

amino acids 585–615 did not impact binding, we performed ITC experiments on the truncated NHR3 (585–615) protein fused to thioredoxin (Trx) for expression, solubility, and stability purposes. We found that the Trx-NHR3(585–615) protein bound to PKA(RIIα) with slightly weaker affinity (K_d = 256 nM) than the entire NHR3 domain (Fig. 1a). To determine whether the Trx fusion affected the binding interaction, we fused full-length NHR3 to Trx and measured binding using ITC. This construct bound 2-fold weaker (K_d = 128 nM) than the wild-type NHR3, indicating that the Trx fusion modestly reduces binding affinity (Fig. 1b). Overall, these results indicate that all the critical binding determinants are retained in the 585–615 construct that we employed for structural studies.

The solution structure of the NHR3(585–615)–PKA(RIIα) complex was calculated using nuclear Overhauser enhancements (NOEs), chemical shifts, and residual dipolar couplings (RDCs) without any significant constraint violations (Table 1). An ensemble of the 15 lowest-energy structures reveals well-defined NHR3(585–615) and PKA(RIIα) (Fig. 2a). An r.m.s.d. value of 0.58 Å was obtained for backbone residues 5–42 of protomers A and B, and for backbone residues 589–613 of NHR3 (Table 1). The NHR3(585–615) subunit forms an amphipathic α-helix when in complex with the PKA(RIIα) dimer (Fig. 2b–d). NHR3(585–615) begins with an extended N-terminal region of five residues, including A585-V589. The structure then continues into a turn dictated by a proline at position 590, and then into a straight helical rod spanning residues E593-Q613, with a two-residue unstructured region at the C-terminus. The RIIα domain of PKA in complex with NHR3(585–615) forms an X-type four-helix bundle (Fig. 2b–d), as shown previously for PKA(RIIα) alone, as well as for PKA(RIIα) bound to Ht31 or AKAP79.[27,28] Each protomer (protomer A: residues 2–44; protomer B: residues 2–44) begins with a short extended region of four residues (residues 2–5; A and B) at the N-terminus, followed by a turn generated by two sequential prolines. The structure then continues into a helix–turn–helix motif, where the N-terminal helix is 14 residues in length (residues 9–22; A and B),

Fig. 1. The NHR3 domain of AML1-ETO specifically binds PKA(RIIα). ITC measurements of the binding of Trx-NHR3 constructs to PKA(RIIα). In each panel, the top portion represents raw data, and the bottom portion is a plot of the binding corrected for dilution enthalpy (squares: experimental data; line: fit to a one-site binding model). The average N (stoichiometry) and K_d values from two independent experiments (±SD) for each protein are shown in the box. (a) ITC of the N-terminal Trx-NHR3 (585–615) construct. (b) ITC of the wild-type Trx-NHR3 (585–654) construct.

Table 1. NMR and refinement statistics for the NHR3(585–615)–PKA(RIIα) complex protein structure

NMR distance and dihedral constraints	NHR3 (585–615)	PKA(RIIα)[a]	
Distance constraints [NOEs (total): 3094]			
Intraresidue	379	908	
Interresidue			
Sequential ($\|i-j\|=1$)	173	516	
Medium range ($1<\|i-j\|<5$)	84	280	
Long range ($\|i-j\|>4$)	6	239	
Intermolecular	294	179	
Ambiguous	NA	42	
Total dihedral angle restraints [Φ (total): 83; Ψ (total): 83]			
Φ	21	62 (31 per monomer)	
Ψ	21	62 (31 per monomer)	
RDCs			
		Monomer I	Monomer II
$^1D_{HN}$ (50+M)	18	22	17
$^1D_{NC'}$ (50+M)	21	21	21
$^1D_{C'Ca}$ (50+M)	22	19	18
$^2D_{HNC'}$ (50+M)	19	NA	
$^1D_{HN}$ (50±MA)	18	NA	
$^1D_{NC'}$ (50±MA)	21	NA	
$^1D_{C'Ca}$ (50±MA)	18	NA	
$^2D_{HNC'}$ (50±MA)	19	NA	

Structure statistics

Violations (mean±SD) [structures: 15]		
Distance constraints (Å)	0.0110±0.0007	
Dihedral angle constraints (°)	0.2709±0.0333	
RDCs (Hz)		
HN (50+M)	1.76±0.07	
NC′ (50+M)	0.79±0.04	
C′C$^\alpha$ (50+M)	0.66±0.04	
HNC′ (50+M)	2.46±0.09	
HN (50±MA)[b]	1.30±0.17	
NC′ (50±MA)[b]	0.37±0.04	
C′C$^\alpha$ (50±MA)[b]	0.40±0.04	
HNC′ (50±MA)[b]	1.32±0.07	
Deviations from idealized geometry		
Bond lengths (Å)	0.0027±0.0001	
Bond angles (°)	0.4223±0.0085	
Impropers (°)	0.2764±0.0152	
Ramachandran plot statistics		
	Rigid regions[c] (%)	Complete structure[d] (%)
Residues in most favored regions	93.2	85.8
Residues in additionally allowed regions	5.5	10.6
Residues in generously allowed regions	0.5	2.3
Residues in disallowed regions	0.8	1.3
Average pairwise r.m.s.d.		
	Rigid regions[c] (Å)	Complete structure[d] (Å)
Heavy	1.45±0.09	2.09±0.18
Backbone	0.58±0.09	1.46±0.28

NA, not available.

All statistics are based on complex structure.

[a] Numbers include both monomers of PKA(RIIα).

[b] Zwitterionic dodecylphosphocholines were included for the NHR3 structure only.

[c] Statistics applied in structure rigid regions (amino acids 11–48, 111–148, and 212–236).

[d] Statistics applied in the total structure (amino acids 8–50, 108–150, 208–238).

the turn (containing two sequential prolines) is 5 residues in length, and the C-terminal helix is 15 residues in length (residues 28–42; A and B). The helices in each monomer are aligned nearly orthogonally to one another, with an interhelical angle of ~118°. The protomers of the PKA(RIIα) dimer are

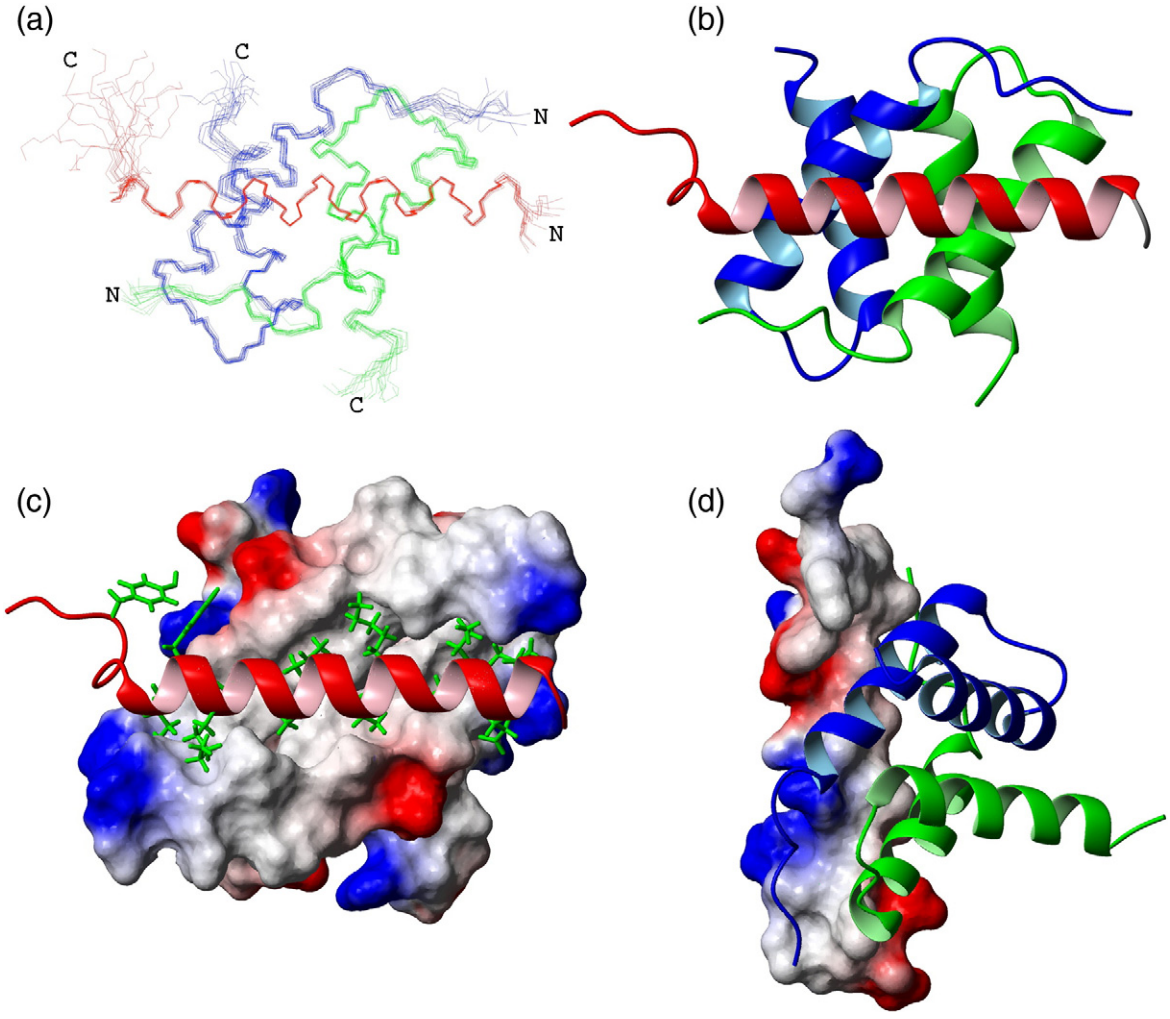

Fig. 2. Solution structure of the NHR3–PKA(RIIα) complex. (a) Overlay of an ensemble of the 15 lowest-energy NMR solution structures. The backbone residues A585-A615 of the NHR3 domain of AML1-ETO (red) and wild-type PKA (RIIα) protomer 1 (blue) and protomer 2 (green) are displayed after superimposing the structures using residues I11-R48 and I111-A148 of PKA(RIIα) and residues V589-Q613 of NHR3. (b) Ribbon representation of the lowest-energy structure. Blue and green represent promoters 1 and 2 of PKA(RIIα), respectively, and red represents the NHR3 domain. (c) Surface representation of the PKA(RIIα) dimer with a ribbon representation of NHR3 (white: nonpolar residues; red: acidic residues; blue: basic residues). The white surface represents the solvent-exposed hydrophobic residues of PKA(RIIα). These residues form a pocket where the hydrophobic residues from NHR3 (green) become buried and make contacts with PKA(RIIα). (d) Surface representation of NHR3 with a ribbon representation of PKA(RIIα) (white: nonpolar residues; red: acidic residues; blue: basic residues).

oriented anti-parallel with one another. More specifically, the N-terminal helix for protomer A is aligned anti-parallel with the N-terminal helix of protomer B, with an interhelical angle of ~174°. The C-terminal helices of each protomer are also aligned anti-parallel, but with an interhelical angle of 135°. This orientation creates an extensive ordering of hydrophobic residues in the core of the four-helix bundle. In addition, a solvent-exposed hydrophobic groove is created on the surface of the molecule between the N-terminal helices of both protomers (Fig. 2c). Our structure of PKA(RIIα) in complex with NHR3(585–615) generally agrees with previously reported structures of PKA(RIIα) complexed with other AKAPs.[27]

Basis for PKA(RIIα) binding to the NHR3 domain

The interaction of the NHR3 domain with PKA (RIIα) is driven principally by hydrophobic interactions with no apparent salt bridge formation (Fig. 2c and d). In addition, there are several polar contacts formed at the binding interface. The hydrophobic groove located on the surface of the N-terminal

helices of PKA(RIIα) is formed by L9 of protomer A, as well as by residues T10, L13, Q14, T17, V18, L21, and R22 of each protomer (Fig. 3a). There are additional contacts made through the N-terminal extended regions of PKA(RIIα). Specifically, I3 and I5 from both protomers make contacts with NHR3. I3 of protomer A makes hydrophobic contacts with I593 and K596 of NHR3, while I5 makes contacts with K596 and A600 and is highly ordered. I3 of protomer B makes contacts with M609 and L612, and I5 makes contacts with M609 and K605, but does not have the same kind of ordering as I5 in protomer A. Residues forming intermolecular interactions from the amphipathic helix of NHR3(585–615) to both N-terminal helices of PKA(RIIα) include I593, W594, A597, A600, V601, V604, A609, and L612 (Fig. 2c and d). In particular, residues V601 and V604 are deeply embedded in the hydrophobic pocket of PKA(RIIα) (Fig. 3a). The methyl groups of V601 are aligned nearly parallel with the N-terminal helix of PKA protomer B, allowing them to make strong hydrophobic contacts with the methyl groups of T10 and T17, the methyl groups of L13, and the aliphatic protons from the side chains in Q14, all of which reside on the N-terminal helix of protomer B. Meanwhile, V604 is aligned nearly

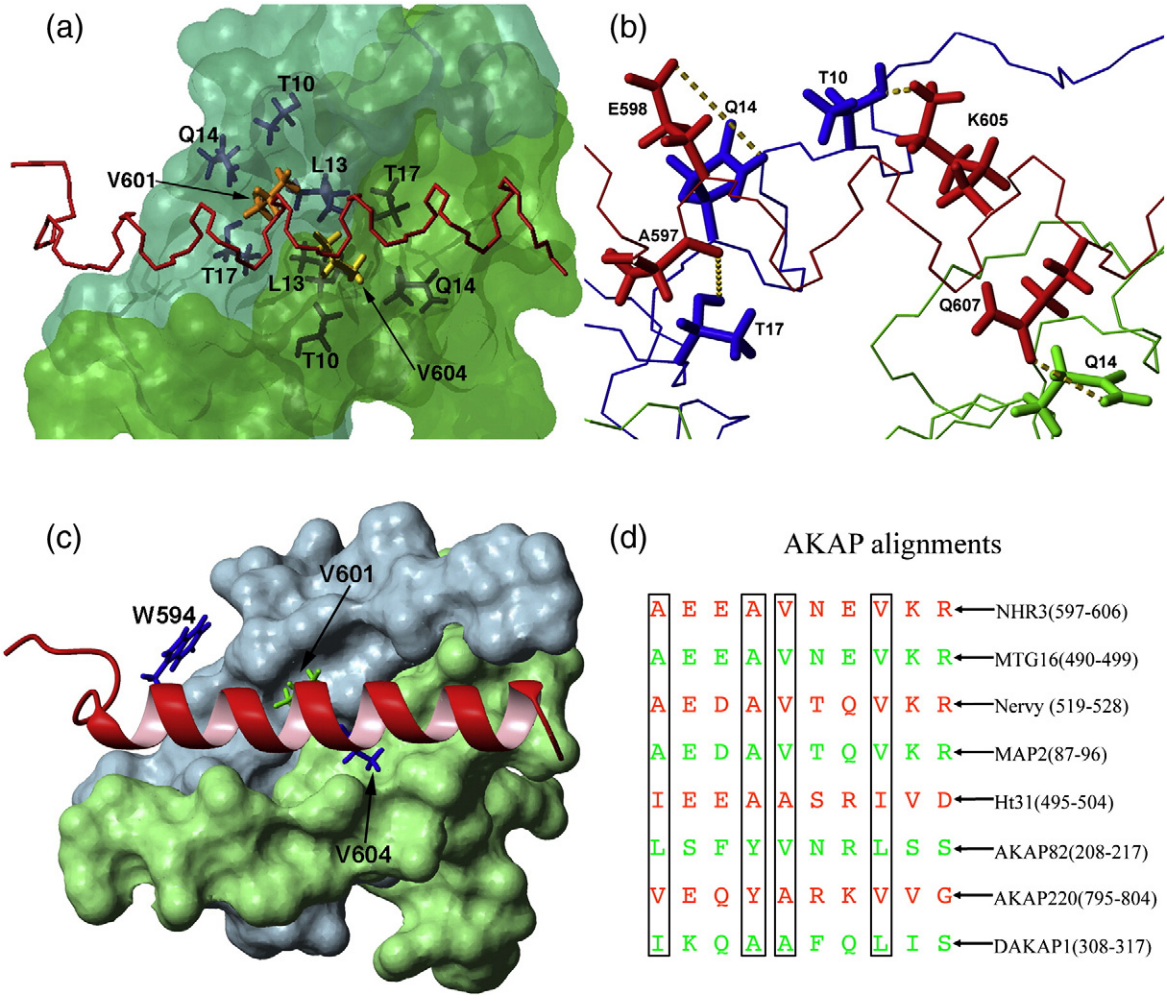

Fig. 3. Residues important for NHR3/PKA(RIIα) binding. (a) Surface representation of the PKA(RIIα) dimer (blue: protomer 1; green: protomer 2) with a line representation of NHR3 (red). Residues that form hydrophobic pockets in PKA (RIIα) are shown in dark-blue and dark-green line representations. Residues V601 and V604 of NHR3 are shown in orange and yellow, respectively. (b) Line representation of PKA(RIIα) dimer (blue: protomer 1; green: protomer 2) with a line representation of NHR3 (red). Hydrogen bonds formed between PKA(RIIα) and NHR3 residues are shown as yellow dotted lines. (c) Surface representation of the PKA(RIIα) dimer (blue: protomer 1; green: protomer 2) with a ribbon representation of NHR3 (red). Residues in NHR3 selected for alanine mutations are highlighted. (d) Alignment of AKAP homologues, including the NHR3 domain of ETO and other ETO homologs. Residues important to the PKA(RIIα) interaction are shown in boxes.

perpendicularly to the N-terminal helix of protomer A and makes similar extensive contacts with the same residues in protomer A of the dimer, suggesting that the two valines are equally important to the interaction (Fig. 3a). V589 from the N-terminal extended region also makes contacts with the N-terminus of one of the two PKA subunits. In addition, the charged and hydrophilic residues K596, K605, and Q613 are also in proximity to PKA(RIIα). While Q613 only makes contacts through the α and β positions, hydrogen bonds form between the side chains of K596 and the side chains of I3 (data not shown) of protomer A, and between the side chains of K605 and the side chains of T10 of protomer B. A hydrogen bond is also formed between the side chain of residue R22 of protomer B and the backbone oxygens of residues G587 and Y588 (data not shown), which are located in the extended region of NHR3, explaining the significance of this region in helping to stabilize the interaction. Hydrogen bonds are also observed between the side chains of E598 and the side chains of Q14 of protomer B, between the side chains of Q607 and the side chains of Q14 of protomer A, and between the backbone oxygen of A597 and the side chain of T17 of protomer B (Fig. 3b). The remaining residues form the hydrophilic side of the amphipathic helix and make no contacts with the PKA (RIIα) dimer. A total surface area of ~1059 Å^2 located on PKA(RIIα) and NHR3(585–615) is buried upon binding of the NHR3 domain. This is comparable to the interaction between Ht31/AKAP79 and PKA(RIIα), where 800 Å^2 of surface area located on PKA(RIIα) is buried, as well as to the interaction between D-AKAP2 and the regulatory subunit of type I cAMP-dependent protein kinase A (PKA (RIα)), where ~710 Å^2 of the hydrophobic groove located on PKA(RIα) is buried.[27,29] While a smaller area of the PKA(RIα) dimer is buried by D-AKAP2, which has a similarly sized helix as NHR3, the decrease in binding surface may be explained by the fact that NHR3 makes contacts with PKA(RIIα) not only through the helix but also through residues located in the N-terminal extended region. D-AKAP2's interaction with PKA(RIα) occurs at a binding affinity (K_d = 48 nM) comparable to that of the interaction between NHR3 and PKA(RIIα), consistent with the similarity in binding surface.[30] However, D-AKAP2 binds PKA(RIIα) with a K_d of 2 nM, ~30-fold higher than NHR3, suggesting that specific residues involved in the AKAP sequences are important for PKA isoform specificity.[30] The flexible unstructured N-terminal regions in RIIα allow for higher-affinity binding and the ability to bind multiple AKAP sequences.[31] In contrast, the rigid N-terminal helices found on RIα allow high-affinity binding of only certain AKAP sequences and at lower affinity compared to RIIα.[31]

Mutation in the NHR3 domain that attenuates PKA(RIIα) binding

Based on the complex structure, we generated mutations in NHR3(585–615) to disrupt its interaction with PKA(RIIα), with the ultimate goal of determining the importance of PKA(RIIα) association for AML1-ETO function. Residues in NHR3 that were shown to be in intimate contact with PKA(RIIα) were selected as possible energetic hot spots important to the protein–protein interaction (Fig. 3c). We observed that W594 (which is conserved with the other mammalian ETO homologues MTG16 and MTGR1, but not with *Drosophila* nervy) interacts with both V18 and Q14 in the N-terminal helix of protomer B of PKA (RIIα), and with V589 in the N-terminal extended region of NHR3. Mutation of W594 to an alanine could potentially disrupt binding to PKA(RIIα) and destabilize the end of the NHR3 helix. As stated above, the highly conserved residues V601 and V604 in NHR3 make multiple contacts deep inside the hydrophobic pocket of PKA(RIIα). V601 and V604 are positioned on either side of the NHR3 helix and contact identical residues from each N-terminal helix of PKA(RIIα), making them strong candidates for point mutations that might attenuate binding (Fig. 3a). The equivalents of both V601P and V601A mutations in the ETO homologue MTG16 were previously shown to disrupt PKA(RIIα) binding (Fig. 3d).[32] We individually substituted all three of these amino acids (W594, V601, and V604) with alanine (Fig. 3c) and performed CD spectroscopy to examine the NHR3 domain's secondary structure (Supplementary Fig. 2). The binding affinities of the mutant NHR3 domains for PKA(RIIα) were measured by ITC and compared to that of the wild-type NHR3 domain (Figs. 1a and 4a–c). The V604A mutant is the only mutant that showed a significant change in the secondary structure, consisting of an increase in helical content (Supplementary Fig. 2). However, this mutation did little to disrupt the binding affinity for PKA(RIIα) (K_d = 383 nM) (Fig. 4b). On the other hand, the CD spectra of the W594A and V601A mutants showed little change compared with the wild-type protein, indicating that these mutations cause no significant change in secondary structure (Supplementary Fig. 2). The binding of the W594A mutant to PKA(RIIα) was impaired only modestly, by approximately 4-fold (K_d = 909 nM) (Fig. 4a). Binding of the V601A mutant, on the other hand, was impaired by approximately 55-fold (K_d = 14 μM), making this a useful mutation for functional studies (Fig. 4c).

Contribution of the NHR3–PKA(RIIα) interaction to AML1-ETO's ability to inhibit granulocyte differentiation

We introduced the V601A mutation into full-length AML1-ETO (Fig. 5a) and assessed the

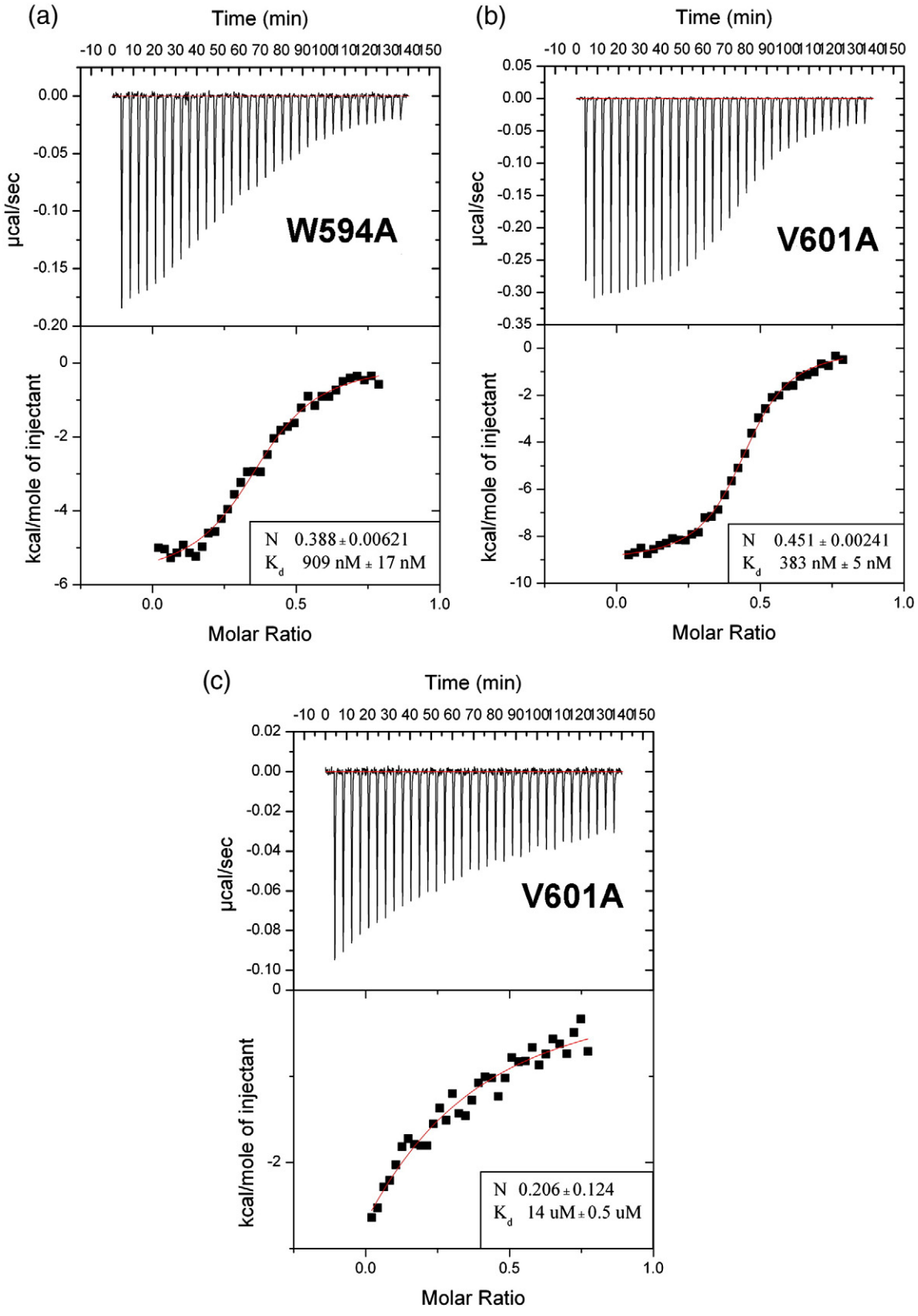

Fig. 4 (*legend on next page*)

protein's ability to interact with PKA(RIIα) upon overexpression in Cos7 cells. The V601A mutation decreased the interaction of AML1-ETO with PKA (RIIα) by approximately 2-fold (Fig. 5b), as measured in titration experiments (data not shown). Since AML1-ETO can form mixed oligomers with wild-type ETO and its family members MTG16 and MTGR1,[10,33] all of which have intact NHR3 domains, PKA(RIIα) could be bound by these mixed oligomers. We therefore performed coimmunoprecipitations with a monomeric form of AML1-ETO that has seven mutated residues in the NHR2 oligomerization domain (m7).[10] The V601A mutation in the context of monomeric AML1-ETO (m7 V601A) decreased the amount of coimmunoprecipitated protein by 3-fold to 4-fold relative to the m7 mutant alone (Fig. 5b). These relatively small perturbations in binding could be due to the presence of additional proteins in cellular extracts that might stabilize the interaction of PKA(RIIα) with the NHR3 domain.

We transduced primary lineage-depleted (Lin^-) mouse BM cells with retroviruses expressing green fluorescent protein (GFP) alone (MigR1), AML1-ETO, or AML1-ETO with V601A substitution in the NHR3 domain, and assessed granulocyte differentiation. The V601A mutation did not significantly affect AML1-ETO's ability to repress granulocyte differentiation, as measured by the percentage of $Gr\text{-}1^+Mac\text{-}1^+$ cells after 7 days of *in vitro* culture in the presence of IL-3, IL-6, stem cell factor (SCF), and granulocyte colony-stimulating factor (Fig. 5c). The m7 mutation, which creates an AML1-ETO monomer, partially ameliorated AML1-ETO's inhibition of granulocyte differentiation, as shown previously.[10] When the V601A mutation was combined with m7, it did not significantly improve granulocyte differentiation, as compared to the m7 mutation alone (Fig. 5c and d). We conclude that an *in vitro* 55-fold reduction of PKA(RIIα) binding to the NHR3 domain does not significantly affect AML1-ETO's ability to repress granulocyte differentiation.

Contribution of the NHR3–PKA(RIIα) interaction to AML1-ETO's ability to inhibit short-term proliferation and long-term self-renewal

AML1-ETO represses the short-term proliferation of human and mouse primary BM cells.[11,34] We introduced MigR1-expressing GFP and wild-type AML1-ETO or the V601A mutant into Lin^- BM cells and measured proliferation 48 h later by BrdU incorporation (Fig. 5e). The V601A mutation did not release the proliferation block imposed by AML1-ETO (Fig. 5e and f).

AML1-ETO increases the clonogenicity of primary BM cells; as a result, cells transduced with AML1-ETO can be serially replated for several weeks *in vitro*.[6,10,11,34] The self-renewal activity of AML1-ETO correlates with its ability to promote leukemia.[7] We transduced Lin^- BM cells with retroviruses expressing wild-type AML1-ETO or AML1-ETO V601A, cultured them, and replated them weekly in the presence of IL-3, IL-6, and SCF. The V601A mutation did not eliminate AML1-ETO's ability to confer an increased self-renewal capacity on hematopoietic progenitors *ex vivo* (Fig. 5g). The number of colonies regenerated on rounds 2 and 4 of replating was, however, significantly lower than that for cells expressing wild-type AML1-ETO, suggesting that the interaction with PKA(RIIα) (or another protein that requires V601 to bind the NHR3 domain) may contribute to a small amount of AML1-ETO's activity.

Effect of the V601A mutation on AML1-ETO + TEL-PDGFβR-induced leukemia

Full-length AML1-ETO can cooperate with activated forms of PDGFβR (TEL-PDGFβR) and FLT3 to generate AML in mice.[5,7,35] We retrovirally transduced BM cells from 5-fluoruracil-treated mice with AML1-ETO and the V601A mutant + TEL-PDGFβR to assess the contribution of PKA (RIIα) binding to leukemogenesis (Fig. 6a). The retrovirus expressing AML1-ETO produced GFP from an internal ribosome entry site, and the TEL-PDGFβR virus produced hCD4. The percentages of doubly transduced cells (GFP^+hCD4^+) were similar for AML1-ETO and the V601A mutant at 2 days postinfection (data not shown). We transplanted lethally irradiated primary recipient animals with 1×10^6 retrovirally transduced, unsorted cells and monitored the animals for disease. The AML that develops in mice transplanted with BM cells expressing both AML1-ETO and TEL-PDGFβR is marked clinically by splenomegaly, hepatomegaly, thrombocytopenia, and anemia, with accumulation of myeloid blasts in the BM and infiltration thereof in the spleen and liver.[5] TEL-PDGFβR will independently generate a chronic myeloproliferative disorder marked by splenomegaly, hepatomegaly, and neutrophilic leukocytosis following a longer latent period.[36]

Fig. 4. NHR3 mutations impair PKA(RIIα) binding. (a) ITC for binding of W594A Trx-NHR3(585–615) to PKA(RIIα). The data numbers presented are averages with standard deviations from two independent runs. Eight-microliter injections were made at 25 °C. K_d and stoichiometry (N) values are indicated in the box. (b) ITC for binding of V604A Trx-NHR3(585–615) to PKA(RIIα), performed as described in (b). (c) ITC for binding of V601A Trx-NHR3(585–615) to PKA(RIIα), performed as described in (b).

Mice transplanted with BM cells expressing both AML1-ETO and TEL-PDGFβR developed a rapid, completely penetrant lethal leukemia, as reported previously,[5,7] and succumbed to their disease within 7 weeks (Fig. 6b). Diseased mice presented with anemia, splenomegaly, and pale livers (data not shown). Mice transplanted with cells expressing TEL-PDGFβR alone, on the other hand, developed a chronic myeloproliferative disorder after a significantly longer latent period. GFP^+hCD4^+ BM cells from mice transplanted with cells expressing AML1-ETO + TEL-PDGFβR contained significantly higher percentages of $c\text{-}kit^+Sca\text{-}1^+$ cells than those transplanted with cells expressing TEL-PDGFβR alone (Fig. 6c and d). The percentage of $Gr\text{-}1^+Mac\text{-}1^+$ cells in the GFP^+hCD4^+ BM population and the intensity of Gr-1 staining were correspondingly lower in the AML1-ETO + TEL-PDGFβR group, reflective of impaired granulocyte differentiation and consistent with a diagnosis of AML (Fig. 6c and e). The AML1-ETO V601 mutant (+TEL-PDGFβR) caused AML with a similar latent period as AML1-ETO. There was a moderate decrease in the percentage of $c\text{-}kit^+Sca\text{-}1^+$ cells, but the cell surface expressions

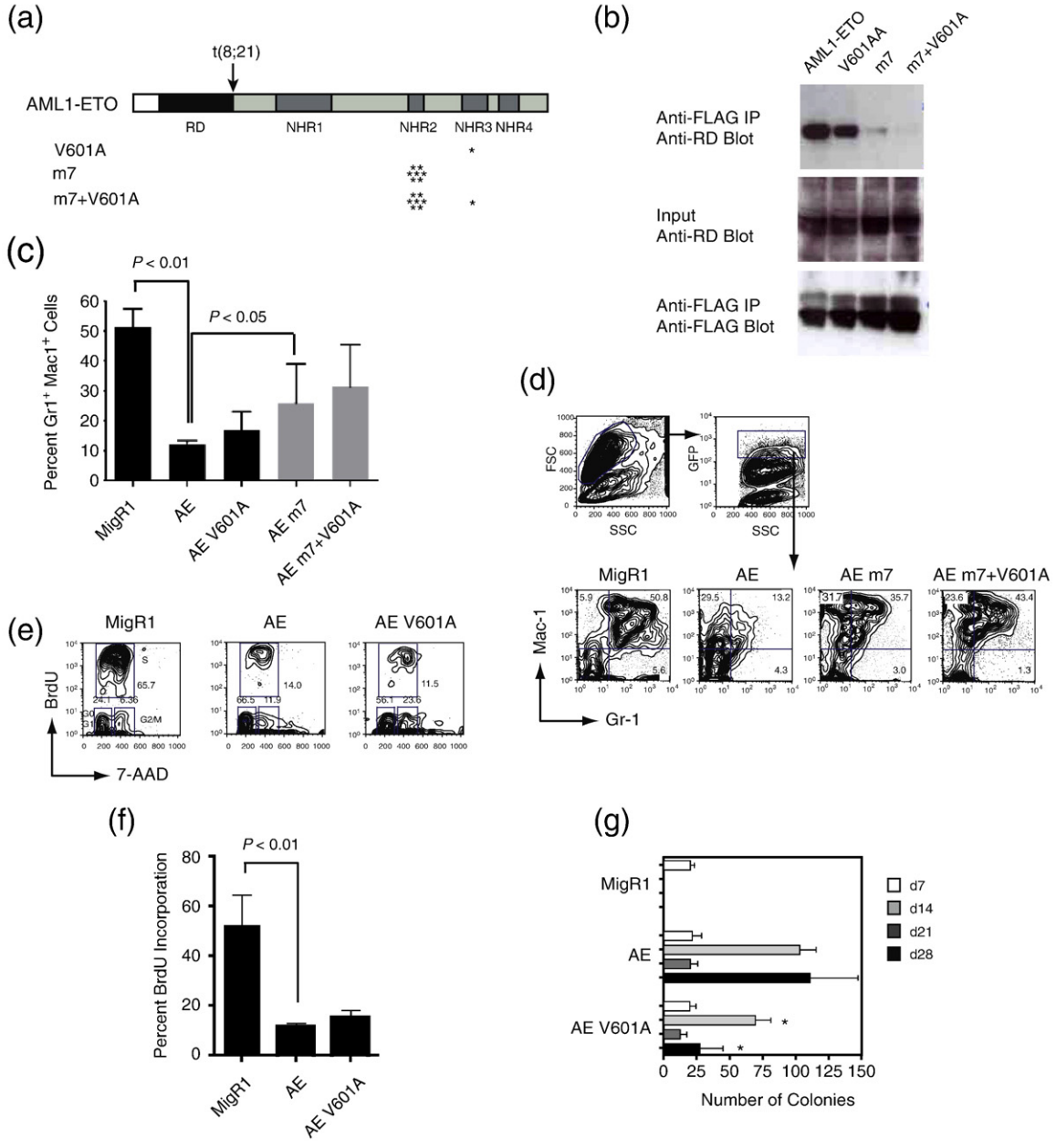

Fig. 5 (*legend on next page*)

of Gr-1 and Mac-1 were not significantly different (Fig. 6c–e). Along with serial replating data, these results suggest that the V601 mutation only very modestly affects AML1-ETO's activity.

In summary, cells expressing AML1-ETO + TEL-PDGFβR gave rise to rapid AML, as reported previously,[5,7] and this was not ameliorated by the V601A mutation.

Discussion

Previous studies identified PKA(RIIα) as an AML1-ETO-interacting protein that binds the NHR3 domain.[4] We solved the structure of the NHR3 domain in a complex with PKA(RIIα). We show that the NHR3 domain forms an amphipathic α-helix when bound to PKA(RIIα), in agreement with other studies on AKAP binding.[27] NHR3 makes extensive contacts with PKA(RIIα) through residues at positions A597, A600, V601, and V604, and makes additional contacts through K605 A608, M609, and L612. Other AKAPs contain hydrophobic residues at similar positions that are important for PKA(RIIα) interaction (Fig. 3d).[27] In addition, K605 forms a hydrogen bond with residue T10 on protomer B of PKA(RIIα). We also observe the interactions of NHR3 residues I593, W594, K596, and Q613 with PKA(RIIα). These residues lengthen the NHR3 helix several turns beyond the AKAP structures observed in other studies, suggesting that the AKAP constructs used in other studies were not long enough and caused the helical fraying at the C-terminus observed in those structures.[27] Residues in the N-terminal extended region also make multiple contacts with PKA(RIIα) through hydrophobic interactions (V589) and formation of hydrogen bonds (G587 and Y588 to R22 of protomer B), suggesting that this region may also contribute to binding.

While the AKAPs do not share a conserved amino acid sequence, they do have a consensus amphipathic helical structure (Fig. 3d).[19,37] This may explain why certain AKAPs can interact with the different isoforms of PKA and also seem to bind PKAs in different structural conformations.[29] The amphipathic helical structure is obviously the main driver of these interactions; however, the amino acid sequence, along with the strategic placement of certain branched hydrophobic residues, seems to dictate PKA specificity, as well as subtle differences in the structure of the PKA–AKAP complex.[29] This is especially evident in the case of D-AKAP2, a dual AKAP that can interact with either the PKA(RIIα) isoform or the PKA(RIα) isoform. Interestingly, D-AKAP2 interacts with both isoforms, as stated above, but there are distinct differences in the complex structures not only due to the structural differences of the PKA isomers but also due to the change in the helical register of the AKAPs.[29,31] It was observed that, during its interaction with PKA (RIIα), D-AKAP2 indeed fitted tightly into the hydrophobic groove; however, in contrast to the complex structure of Ht31 bound to PKA(RIIα), only one of the flexible N-terminal regions of the A protomer is shown to interact with the AKAPs, while the other N-terminal region from the second protomer remains flexible and disordered and ultimately does not participate in the interaction.[29,31] This may explain how PKA(RIIα) is able to recognize different AKAP sequence motifs while maintaining high-affinity interactions, consistent

Fig. 5. AML1-ETO is unaffected by mutations that impair PKA(RIIα) binding. (a) Schematic diagram of AML1-ETO and the location of mutations (asterisks) that disrupt oligomerization (m7) and the binding of PKA(RIIα) (V601A). (b) Cos7 cells were cotransfected with AML1-ETO and its mutated derivatives, along with FLAG-tagged PKA(RIIα). Top: Cell lysates immunoprecipitated (IP) with anti-FLAG and blotted with antibody to the Runt domain (RD) in AML1-ETO. Middle: 10% of input lysate blotted with anti-RD to detect AML1-ETO proteins. Bottom: Membranes from the top panel were reprobed with anti-FLAG antibodies. (c) Effect of mutations on AML1-ETO's (AE) repression of the granulocyte differentiation of primary Lin^- BM cells following 7 days of culture in the presence of IL-3, IL-6, SCF, and granulocyte colony-stimulating factor. Plotted are triplicate samples from two independent experiments ($n = 6$). Error bars represent 95% confidence intervals. Significant differences from AE are shown (ANOVA and Dunett's multiple comparison test). (d) Granulocyte differentiation as assessed by the percentage of $Gr\text{-}1^+Mac\text{-}1^+$ cells. Cells within the forward-scatter and side-scatter gates were further gated for GFP expression, and GFP^+ cells were examined for Mac-1 and Gr-1 expression. The V601A mutation did not significantly attenuate either the activity of AE or the activity of the AE m7 mutant. The data are included in the summary graph in (c). (e) Representative flow of BrdU incorporation 48 h after the transduction of Lin^- BM cells with MigR1 expressing GFP, AE, or the AE V601A mutant. Forward/side scatter and GFP (data not shown) were gated as described in (d). (f) Percentage of GFP^+ cells that had incorporated BrdU following a 1-h BrdU pulse. Data are from two experiments, each with triplicate samples (error bars represent 95% confidence intervals; significance was determined by ANOVA and Dunett's multiple comparison test). (g) Serial replating of BM cells. Graphs represent the average number of colonies from each round of replating in the presence of IL-3, IL-6, and SCF. Day 7 represents colony numbers per 10^3 cells plated; days 14, 21, and 28 represent colony numbers from 1×10^4 plated cells. Numbers are averaged from three experiments, each containing triplicate samples. The number of colonies derived from AE V601A-transduced cells was significantly lower than the number of colonies derived from AE-transduced cells on days 14 and 28 ($P < 0.01$, ANOVA and Dunett's multiple comparison test).

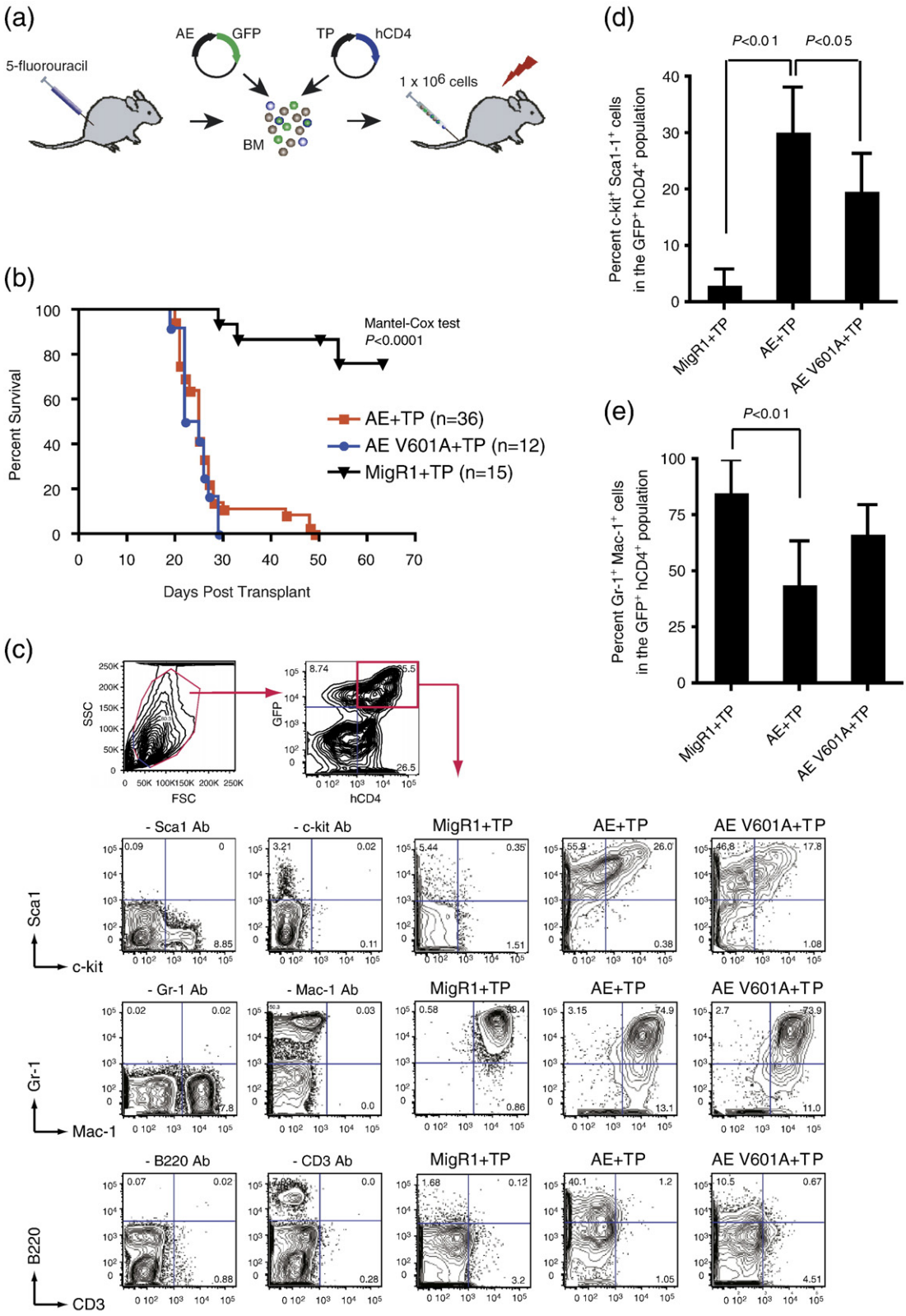

Fig. 6 (*legend on next page*)

with the ubiquitous expression of PKA(RIIα) and its importance in the regulation of many cellular processes during growth and development.[19,20,27,38]

In contrast to the D-AKAP2–PKA(RIIα) complex, we observe that the interaction between NHR3 and PKA(RIIα) resembles the interaction between PKA (RIIα) and Ht31 in that both flexible N-terminal regions of PKA(RIIα) make contacts with the NHR3 helix.[27] As stated above, residues I3 and I5 from both N-terminal regions make contacts with the NHR3 helix. While I3 and I5 from protomer B do make contacts with the NHR3 helix and show partial ordering, the observed NOEs are relatively weak, a possible result of the protonation of the N-terminal histidines that occurs under the pH 4.0 conditions employed for solubility.[27] We observe an extensive ordering of I5 from protomer A, as well as partial ordering of I3. While our experimental conditions may contribute to the partial disordering of this flexible region, it is clear that both N-terminal regions make contacts with the NHR3 helix and contribute to binding, which is a distinction from the D-AKAP2 complex.

The residues identified as essential to the binding interaction are the main difference between our structure and the Ht31/PKA(RIIα) structure. In the previous study, alignments showed that residues at equivalent positions 604 and 605 of NHR3 were identified as essential to the AKAP interaction.[27] The results from our mutagenesis study clearly show that the valine at position 604 does not contribute significantly to PKA(RIIα) binding. Additionally, the lysine at position 605 is not completely buried in the hydrophobic pocket. Small contacts with the hydrophobic core of PKA (RIIα) were observed through the aliphatic portion of the side chain, but the main contacts were observed between the side chain and the N-terminal region of protomer B, and through a hydrogen bond formed with T10 in protomer B of PKA(RIIα). K605 and the hydrogen bond may be important for PKA isomer specificity, as alignments with other AKAPs generally contain a hydrophobic residue at this position. Our results show that the valine at position 601 is required for high-affinity binding to PKA (RIIα). This position represents a shift in the helical registry of a full turn when compared to AKAP sequence alignments that show the equivalent of positions 604 and 605 as being necessary to the PKA interaction. These results agree with other studies showing that AKAPs have the ability to bind at different positions along the helical registry, a fact illustrated by D-AKAP2's ability to interact with two PKA isoforms at different helical registries.[29]

Using the structural information, we showed that a 55-fold disruption of binding between the isolated NHR3 domain and PKA(RIIα) *in vitro* did not affect AML1-ETO's *in vivo* leukemogenic activity. The V601A mutation that we introduced into AML1-ETO only modestly disrupted PKA (RIIα) binding (3-fold to 4-fold) in cell extracts, potentially raising the concern that we have not sufficiently impaired binding to cause an *in vivo* effect. This scenario is well illustrated by recent studies that examined the importance of CBFβ binding to AML1-ETO, in which mutations that decreased CBFβ binding by approximately 50-fold had little effect on AML1-ETO's leukemogenic activity, whereas a >400-fold decrease in affinity severely impeded leukemogenesis.[6,7,39] Another possible concern is that AML1-ETO can recruit PKA(RIα) through the RI specifier region (RISR) motif, as this was observed to be the case in the MTG16b homologue of ETO.[40,41] A sequence alignment of AML1-ETO with other proteins containing the RISR motif shows that AML1-ETO does in fact contain a RISR motif in the NHR3 domain just C-terminal to the AKAP site (Fig. 7). This could allow AML1-ETO to recruit a different PKA R isoform even though the V601A mutant interrupts binding to PKA(RIIα). It is also possible that the AKAP site in NHR3 could bind both isoforms of PKA R subunits, as is the case with D-AKAP2.[29,31] Therefore, the V601A mutation could inhibit the interaction with the RIIα isomer, while still allowing the interaction with RIα to occur.

Fig. 6. The V601A mutation in AML1-ETO does not impair its leukemogenic activity. (a) Schematic of transplantation protocol. BM mononuclear cells harvested from 5-fluoruracil-treated C57BL/6 mice were coinfected with MigR1 expressing AE (or AE V601A) and TEL-PDGFβR (TP). IRES-mediated expression of GFP marks AE-expressing cells, while hCD4 marks TP-expressing cells. Retrovirally transduced cells (1×10^6) were transplanted along with 2×10^5 normal BM cells into lethally irradiated mice. (b) Kaplan–Meier survival curve of mice after transplantation with retroviruses expressing AE or AE V601A + TP. Control mice expressing MigR1 (+GFP) and TP (+hCD4) are shown. The study end point was 63 days. The number of mice in each group is indicated. (c) Whole BM of diseased mice was gated based on forward-scatter and side-scatter characteristics and subsequently analyzed for the expression of hCD4 (TEL-PDGFβR) and GFP (AML1-ETO). GFP^+hCD4^+ cells were then analyzed for the expression of myeloid and progenitor markers. Plots are from a single animal representative of the experimental group. Dropout antibody controls were performed using normal BM. Although there appears to be a higher percentage of $B220^+$ cells in the AE + TP samples than in the AE V601A + TP samples, this difference was not significant (data not shown). (d) The percentage of GFP^+hCD4^+ BM cells that were positive for both c-kit and Sca-1. Error bars indicate 95% confidence intervals. AE + TP, $n=9$ mice; V601A + TP, $n=8$; MigR1 + TP, $n=7$. Differences relative to AE + TP were determined using Dunett's test and ANOVA. (e) Differences in the percentages of GFP^+hCD4^+ BM cells that were positive for both Gr-1 and Mac-1, analyzed as in (d).

Fig. 7. Alignment of RISR sequences and NHR3 domain. Amino acids 618–647, directly C-terminal to NHR3(585–615), shows homology to other RISRs that have been identified. Residues in red have been shown to be functionally conserved.

Point mutations of certain branched hydrophobic residues induced changes in the binding affinity of one PKA R isomer while having little effect, or the opposite effect, on the other.[29,31] This is unlikely, as alignments of the NHR3 AKAP site to D-AKAP2 do not meet the criteria for dual specificity established by Sarma *et al.*, as two charged residues align with positions reserved for hydrophobic residues. Regardless, previous studies showed that deletion of the entire NHR3 domain did not impair the serial replating ability conferred by AML1-ETO on the primary BM cells.[8] The ability to confer serial replating *ex vivo* is a useful surrogate for the *in vivo* self-renewal and leukemogenic activity conferred by oncogenic nuclear proteins.[6,7,42–45] Thus, we can reasonably conclude, as have others,[8] that proteins interacting with NHR3 contribute very little to AML1-ETO's leukemogenic activity.

Several studies showed that a truncation that removes both the NHR3 domain and the NHR4 domain augments AML1-ETO's leukemogenic activity, enabling it to cause disease in the absence of an experimentally induced secondary mutation.[17,18] NHR4 appears to be largely responsible for this dampening of AML1-ETO's leukemogenic activity, as a mutation that unfolds the domain had the same effect as removing NHR3 and NHR4.[16] We did not directly assess whether the V601A mutation in NHR3 augmented AML1-ETO's leukemogenic activity in the absence of an experimentally induced second hit; thus, this remains an open question. However, given the observation that the AML1-ETO V601A mutation significantly decreased the percentage of c-kit$^+$ cells in the BM of leukemic mice, we predict that the interaction with PKA (RIIα) will not actively block AML1-ETO's activity.

It has been proposed that ETO and the related MTG16 proteins are AKAPs based on their interaction with PKA(RIIα).[4,32,41] We show that the NHR3 domain indeed directly binds PKA(RIIα) with high affinity. AKAPs are located in several subcellular compartments and participate in multiple signaling pathways.[22] Although we did not demonstrate a role for the NHR3–PKA(RIIα) interaction for AML1-ETO-mediated leukemogenesis, it may be important for normal ETO function. It was recently shown, for example, that mammalian MTG16b (an ETO homologue and AKAP found in immune cells) interacts with plexins A1 and A3, as well as with both type I and type II PKAs, thus forming a signaling complex.[41] This study observed that phosphorylation of plexin A3 by type I PKA increased the interaction with MTG16b. This is significant because it suggests the possibility that the interaction of MTG16b and PKA is involved in cAMP targeting and in the integration of semaphorin signaling in immune cells. In addition, it was reported that the *Drosophila* ETO homologue nervy interacts at the plasma membrane with plexin A, a receptor for semaphorin.[46] Nervy also interacts with PKA, and both nervy and PKA antagonize repulsion mediated by the interaction between semaphorin and plexin A. Nervy with a mutation equivalent to V601P, which would break the NHR3 α-helix and presumably disrupt the domain's structure, could not rescue a nervy loss of function phenotype, indicating that the NHR3 domain is essential for nervy function. The equivalent of a V601A mutation in other AKAPs would represent a reagent that would be useful in a more precise investigation of the interactions of AKAPs with PKA(RIIα) and their functional significance.

Our long-term goal is to identify protein–protein interactions that are essential for AML1-ETO's activity, and then to develop inhibitors that block those interactions.[47] Of the six protein–protein (or protein–DNA) interactions thus far analyzed, only three would appear to be potential targets for small-molecule or peptide inhibitors: the interaction of the Runt domain with DNA and CBFβ, and oligomerization through the NHR2 domain. Higher-order protein complexes formed on AML1-ETO, or proteins that bind to nonconserved domains may also present therapeutic opportunities, but they first require identification and/or validation.

Materials and Methods

Protein expression and purification

NHR3 residues A585-N654 were cloned into both pHis-parallel and pET-32a expression vectors (Novagen, Madison WI) between the BamHI site and the XhoI site using standard PCR cloning methods.[48] Truncated versions of NHR3 A585-A615 and K623-D648 were also cloned into the pET-32a expression vector. Point mutations were introduced into NHR3 constructs using the Quick Change Site-Directed Mutagenesis kit (Stratagene, La Jolla, CA). Wild-type PKA(RIIα) was cloned between the BamHI site and the XhoI site of the pHis-parallel vector. All NHR3 constructs, as well as PKA(RIIα), were expressed in Rosetta (DE3)-competent cells. Cells were induced at 30 °C using 0.8 mM IPTG at an OD_{600} of 0.6–0.8. NHR3 constructs and PKA(RIIα) were purified separately using the same protocols. Cells were incubated at 4 °C in the presence of ethylenediaminetetraacetic acid

(EDTA)-free protease inhibitors (Roche, Indianapolis, IN) for 30 min, lysed by three passes through a French press, and clarified by centrifugation. The supernatant was applied to a Ni-NTA column (Qiagen, Valencia, CA); washed with 50 mM Tris–HCl (pH 7.2), 300 mM NaCl, 30 mM imidazole, and 1 mM Pefabloc; and eluted with 50 mM Tris–HCl (pH 7.2), 300 mM NaCl, 250 mM imidazole, and 1 mM Pefabloc. The protein was dialyzed against 50 mM Tris–HCl (pH 7.2), 25 mM NaCl, 1 mM EDTA, and 1 mM DTT to remove imidazole while cleaving the 6×His-tag or Trx-fused His-tag with Ac-TEV (Invitrogen, Carlsbad, CA). The cleaved protein was passed through the Ni-NTA column to remove the His-tag or Trx-fused His-tag. The nonadherent fraction was further purified using Q-Sepharose (GE Healthcare, Piscataway, NJ). For formation of the complex, NHR3 and PKA(RIIα) were dialyzed against 25 mM KPi (pH 6.5), 150 mM KCl, and 1 mM EDTA for 3 h, and then mixed together in a 2:1 PKA(RIIα)/NHR3 ratio. The mixture was incubated at room temperature for 1 h, and then the pH of the solution was rapidly dropped to pH 4.0 and dialyzed against 20 mM NaPi (pH 4.0) and 1 mM EDTA. The protein complex was applied to an S-100 size-exclusion chromatography column (GE Healthcare) to remove any unbound protein.

Isothermal titration calorimetry

ITC experiments were carried out on a VP-ITC MicroCalorimeter system (MicroCal, Inc., Northampton, MA) at 25 °C. Samples were dialyzed against 25 mM KPi (pH 6.5), 150 mM KCl, 1 mM EDTA, and 1 mM DTT, centrifuged to remove any particulates, and degassed. A solution of 18 μM wild-type PKA(RIIα) was titrated with 129 μM wild-type NHR3(585–654). Wild-type PKA(RIIα) (36 μM) was titrated with 124 μM Trx-NHR3(585–654). PKA(RIIα) (27 μM) was titrated with 100 μM Trx-NHR3(585–615), 100 μM Trx-NHR3 (585–615) W594A, 100 μM Trx-NHR3(585–615) V601A, and 100 μM Trx-NHR3(585–615) V604A. Data were corrected for dilution enthalpy and then analyzed using Origin 7.0 (Origin Lab, Northampton, MA).

NMR spectroscopy

All NMR experiments were performed at 30 °C on a Varian Inova 500-MHz spectrometer or a 600-MHz spectrometer (Palo Alto, CA) equipped with a cryoprobe. All NMR samples were prepared in 20 mM NaPi (pH 4.0), 1 mM EDTA, and 5% (vol/vol) D_2O. U-[^{15}N,^{13}C]-labeled NHR3 domain complexed with unlabeled PKA(RIIα) was prepared for conventional triple-resonance experiments and peak assignments for the NHR3 domain. U-[^{15}N,^{13}C]-labeled PKA(RIIα) complexed with unlabeled NHR3 domain was prepared for conventional triple-resonance experiments and peak assignments for PKA(RIIα). A series of half-filtered ^{13}C-edited–^{12}C-filtered/^{13}C-filtered and ^{15}N-edited–^{14}N-filtered/^{15}N-filtered NOE spectroscopy experiments was performed to determine intermolecular NOEs between the two proteins. In addition, a sample consisting of 50% unlabeled PKA(RIIα) and 50% U-[^{15}N,^{13}C] was complexed to an unlabeled NHR3 domain to determine interdimer NOEs, as described previously for studies of PKA(RIIα) complexes with Ht31 and AKAP79.[27] U-[^{15}N,^{13}C]-labeled PKA(RIIα)/unlabeled NHR3 domain and U-[^{15}N,^{13}C]-labeled NHR3 domain/unlabeled PKA(RIIα) were each soaked in a 6% compressed positively charged polyacrylamide gel and a 4% compressed zwitterionic polyacrylamide gel for collection of RDC data.[49] Four types of RDCs—$^{1}D_{HN}$, $^{1}D_{NC'}$, $^{1}D_{C'C^{\alpha}}$, and $^{2}D_{HNC'}$—were measured using HNCO-based experiments.[50]

Structure calculation

Because the symmetry between the two protomers of the PKA(RIIα) dimer is partially broken upon binding with NHR3(585–615), peak splitting in the spectra of the labeled PKA(RIIα) was observed for ~50% of the residues. Since symmetry for the other 50% of the residues remains, it was impossible to assign the two protomers of the PKA (RIIα) unambiguously. Therefore, it was necessary to ambiguously assign all of the residues in the PKA(RIIα) spectra using an assignment nomenclature that included different numbering systems for each protomer of PKA (RIIα) and for the NHR3(585–615) monomer. The assignment nomenclature was as follows: amino acids 1/101–50/150 designate protomer A of PKA(RIIα), and amino acids 101/1–150/50 designate protomer B of PKA(RIIα). Residues 1/101–7/107 and 101/1–107/7 are residuals from the expression vector; therefore, residues 8/108–50/150 or residues 108/8–150/50 correspond to residues 2–44 of PKA(RIIα). The Sparky program allowed for the ambiguous assignment of all NOEs generated by the PKA (RIIα) dimer. Therefore, any NOE generated by the PKA (RIIα) dimer was assigned as being generated by protomer A or protomer B (e.g., Y22/Y122N-Q21/Q121CA-Y22/Y122HN). Assignments for the residues in the NHR3(585–615) portion of the complex were designated 201–237 to further distinguish the different subunits in this trimer. Residues 201–207 are residuals from the expression vector; therefore, residues 208–238 correspond to residues 585–615 of NHR3. While intramolecular NOEs of the NHR3(585–615) were all unambiguously assigned, intermolecular long-range NOEs to PKA(RIIα) were all ambiguously assigned to both protomers of PKA(RIIα).

The structure of the NHR3–PKA(RIIα) complex was calculated with CNS by employing the simulated annealing protocol.[51] NOE restraints were obtained from manual assignment and classified into three groups: 1.8–1.1, 1.8–2.5, and 1.8–3.7 Å. φ and ψ dihedral angle restraints were generated by TALOS prediction based on C^{α}, C^{β}, C′, and N chemical shifts.[52] Eight sets of RDCs ($^{1}D_{HN}$, $^{1}D_{NC'}$, $^{1}D_{C'C^{\alpha}}$, and $^{2}D_{HNC'}$ from each gel condition) were used in the structure calculations. The initial D_a and R values of the alignment tensor were estimated from a histogram of RDC distribution.[53] The 15 lowest-energy structures out of 200 calculated structures were selected to represent the structure.

Retroviral transduction and *in vitro* and *in vivo* assays

Mutated AML1-ETO proteins were prepared using the QuickChange Site-Directed Mutagenesis kit and coding sequences transferred from pBluescript to the MigR1 vector. Retroviruses were prepared and transduced into C57BL/6 mouse BM cells, as described previously.[7,9,10,13]

Granulocyte differentiation assays, serial replating assays, cell cycle kinetics, and leukemogenesis assays were performed as described previously.[7,9,10,13] Mice were monitored for the development of leukemia by observing for physical symptoms characterized by lethargy and splenomegaly. Sick mice were euthanized, and all remaining mice were sacrificed at 63 days. Diagnoses of chronic myeloproliferative disease and AML were based on criteria described previously.[7] All animal work was approved by the Institute Animal Care and Use Committee at Dartmouth.

Flow cytometry

Samples were analyzed either on FACSCalibur or on LSRII (BD Biosciences, San Jose, CA). The antibodies used were as follows: APC-Cy7-conjugated or PE-conjugated anti-Mac-1 (clone M1/70; BD Pharmingen), PerCP-Cy5.5-conjugated or APC-conjugated anti-Gr-1 (clone RB6-8C5; BD Pharmingen), PE-Cy7-conjugated anti-B220 (clone RA3-6B2; eBioscience), APC-conjugated anti-CD3 (clone 145-2C11; BD Pharmingen), PE-Cy7-conjugated anti-Sca1 (clone D7; BD Pharmingen), APC-conjugated anti-CD117 (clone 2B8; eBioscience), and PE-conjugated anti-human CD4 (clone L3T4; eBioscience).

Coimmunoprecipitation

Immunoprecipitation of FLAG-tagged PKA(RIIα) from Cos7 cell extracts and immunoblotting, using anti-FLAG or monoclonal anti-Runt domain antibodies, was performed as described previously.[9]

Accession numbers

Coordinates and structures factors have been deposited at the Biological Magnetic Resonance Bank and the Protein Data Bank under accession codes 16954 and 2kyg.

Acknowledgements

The authors thank Gary Gilliland for the TEL-PDGFβR cDNA and Warren Pear for the MigR1 vector.

Supplementary Data

Supplementary data associated with this article can be found, in the online version, at doi:10.1016/j.jmb.2010.08.007

References

1. Miyoshi, H., Shimizu, K., Kozu, T., Maseki, N., Kaneko, Y. & Ohki, M. (1991). t(8;21) breakpoints on chromosome 21 in acute myeloid leukemia are clustered within a limited region of a single gene, AML1. *Proc. Natl Acad. Sci. USA*, **88**, 10431–10434.
2. Hug, B. A. & Lazar, M. A. (2004). ETO interacting proteins. *Oncogene*, **23**, 4270–4274.
3. Davis, J. N., McGhee, L. & Meyers, S. (2003). The ETO (MTG8) gene family. *Gene*, **303**, 1–10.
4. Fukuyama, T., Sueoka, E., Sugio, Y., Otsuka, T., Niho, Y., Akagi, K. & Kozu, T. (2001). MTG8 proto-oncoprotein interacts with the regulatory subunit of type II cyclic AMP-dependent protein kinase in lymphocytes. *Oncogene*, **20**, 6225–6232.
5. Grisolano, J. L., O'Neal, J., Cain, J. & Tomasson, M. H. (2003). An activated receptor tyrosine kinase, TEL/PDGFbetaR, cooperates with AML1/ETO to induce acute myeloid leukemia in mice. *Proc. Natl Acad. Sci. USA*, **100**, 9506–9511.
6. Kwok, C., Zeisig, B. B., Qiu, J., Dong, S. & So, C. W. (2009). Transforming activity of AML1-ETO is independent of CBFbeta and ETO interaction but requires formation of homo-oligomeric complexes. *Proc. Natl Acad. Sci. USA*, **106**, 2853–2858.
7. Roudaia, L., Cheney, M. D., Manuylova, E., Chen, W., Morrow, M., Park, S. *et al.* (2009). CBFbeta is critical for AML1-ETO and TEL-AML1 activity. *Blood*, **113**, 3070–3079.
8. Yan, M., Ahn, E. Y., Hiebert, S. W. & Zhang, D. E. (2009). RUNX1/AML1 DNA binding domain and ETO/MTG8 NHR2 dimerization domain are critical to AML1-ETO9a leukemogenesis. *Blood*, **113**, 883–886.
9. Park, S., Chen, W., Cierpicki, T., Tonelli, M., Cai, X., Speck, N. A. & Bushweller, J. H. (2009). Structure of the AML1-ETO eTAFH domain–HEB peptide complex and its contribution to AML1-ETO activity. *Blood*, **113**, 3558–3567.
10. Liu, Y., Cheney, M. D., Gaudet, J. J., Chruszcz, M., Lukasik, S. M., Sugiyama, D. *et al.* (2006). The tetramer structure of the nervy homology two domain, NHR2, is critical for AML1/ETO's activity. *Cancer Cell*, **9**, 249–260.
11. Hug, B. A., Lee, S. Y., Kinsler, E. L., Zhang, J. & Lazar, M. A. (2002). Cooperative function of AML1-ETO corepressor recruitment domains in the expansion of primary bone marrow cells. *Cancer Res.* **62**, 2906–2912.
12. Gelmetti, V., Zhang, J., Fanelli, M., Minucci, S., Pelicci, P. G. & Lazar, M. A. (1998). Aberrant recruitment of the nuclear receptor corepressor–histone deacetylase complex by the acute myeloid leukemia fusion partner ETO. *Mol. Cell. Biol.* **18**, 7185–7191.
13. Liu, Y., Chen, W., Gaudet, J., Cheney, M. D., Roudaia, L., Cierpicki, T. *et al.* (2007). Structural basis for recognition of SMRT/N-CoR by the MYND domain and its contribution to AML1/ETO's activity. *Cancer Cell*, **11**, 483–497.
14. Lutterbach, B., Westendorf, J. J., Linggi, B., Patten, A., Moniwa, M., Davie, J. R. *et al.* (1998). ETO, a target of t (8;21) in acute leukemia, interacts with the N-CoR and mSin3 corepressors. *Mol. Cell. Biol.* **18**, 7176–7184.
15. Wang, J., Hoshino, T., Redner, R. L., Kajigaya, S. & Liu, J. M. (1998). ETO, fusion partner in t(8;21) acute myeloid leukemia, represses transcription by interaction with the human N-CoR/mSin3/HDAC1 complex. *Proc. Natl Acad. Sci. USA*, **95**, 10860–10865.
16. Ahn, E. Y., Yan, M., Malakhova, O. A., Lo, M. C., Boyapati, A., Ommen, H. B. *et al.* (2008). Disruption of

the NHR4 domain structure in AML1-ETO abrogates SON binding and promotes leukemogenesis. *Proc. Natl Acad. Sci. USA*, **105**, 17103–17108.
17. Yan, M., Burel, S. A., Peterson, L. F., Kanbe, E., Iwasaki, H., Boyapati, A. *et al.* (2004). Deletion of an AML1-ETO C-terminal NcoR/SMRT-interacting region strongly induces leukemia development. *Proc. Natl Acad. Sci. USA*, **101**, 17186–17891.
18. Yan, M., Kanbe, E., Peterson, L. F., Boyapati, A., Miao, Y., Wang, Y. *et al.* (2006). A previously unidentified alternatively spliced isoform of t(8;21) transcript promotes leukemogenesis. *Nat. Med.* **12**, 945–949.
19. Carnegie, G. K., Means, C. K. & Scott, J. D. (2009). A-kinase anchoring proteins: from protein complexes to physiology and disease. *IUBMB Life*, **61**, 394–406.
20. Beene, D. L. & Scott, J. D. (2007). A-kinase anchoring proteins take shape. *Curr. Opin. Cell Biol.* **19**, 192–198.
21. Cheng, X., Ji, Z., Tsalkova, T. & Mei, F. (2008). Epac and PKA: a tale of two intracellular cAMP receptors. *Acta Biochim. Biophys. Sin. (Shanghai)*, **40**, 651–662.
22. Dessauer, C. W. (2009). Adenylyl cyclase—A-kinase anchoring protein complexes: the next dimension in cAMP signaling. *Mol. Pharmacol.* **76**, 935–941.
23. Taylor, S. S., Buechler, J. A. & Yonemoto, W. (1990). cAMP-dependent protein kinase: framework for a diverse family of regulatory enzymes. *Annu. Rev. Biochem.* **59**, 971–1005.
24. Rubin, C. S. (1979). Characterization and comparison of membrane-associated and cytosolic cAMP-dependent protein kinases. Studies on human erythrocyte protein kinases. *J. Biol. Chem.* **254**, 12439–12449.
25. Luo, Z., Shafit-Zagardo, B. & Erlichman, J. (1990). Identification of the MAP2- and P75-binding domain in the regulatory subunit (RII beta) of type II cAMP-dependent protein kinase. Cloning and expression of the cDNA for bovine brain RII beta. *J. Biol. Chem.* **265**, 21804–21810.
26. Scott, J. D., Stofko, R. E., McDonald, J. R., Comer, J. D., Vitalis, E. A. & Mangili, J. A. (1990). Type II regulatory subunit dimerization determines the subcellular localization of the cAMP-dependent protein kinase. *J. Biol. Chem.* **265**, 21561–21566.
27. Newlon, M. G., Roy, M., Morikis, D., Carr, D. W., Westphal, R., Scott, J. D. & Jennings, P. A. (2001). A novel mechanism of PKA anchoring revealed by solution structures of anchoring complexes. *EMBO J.* **20**, 1651–1662.
28. Newlon, M. G., Roy, M., Morikis, D., Hausken, Z. E., Coghlan, V., Scott, J. D. & Jennings, P. A. (1999). The molecular basis for protein kinase A anchoring revealed by solution NMR. *Nat. Struct. Biol.* **6**, 222–227.
29. Sarma, G. N., Kinderman, F. S., Kim, C., von Daake, S., Chen, L., Wang, B. C. & Taylor, S. S. (2010). Structure of D-AKAP2:PKA RI complex: insights into AKAP specificity and selectivity. *Structure*, **18**, 155–166.
30. Burns, L. L., Canaves, J. M., Pennypacker, J. K., Blumenthal, D. K. & Taylor, S. S. (2003). Isoform specific differences in binding of a dual-specificity A-kinase anchoring protein to type I and type II regulatory subunits of PKA. *Biochemistry*, **42**, 5754–5763.
31. Kinderman, F. S., Kim, C., von Daake, S., Ma, Y., Pham, B. Q., Spraggon, G. *et al.* (2006). A dynamic mechanism for AKAP binding to RII isoforms of cAMP-dependent protein kinase. *Mol. Cell*, **24**, 397–408.
32. Schillace, R. V., Andrews, S. F., Liberty, G. A., Davey, M. P. & Carr, D. W. (2002). Identification and characterization of myeloid translocation gene 16b as a novel A-kinase anchoring protein in T lymphocytes. *J. Immunol.* **168**, 1590–1599.
33. Kitabayashi, I., Ida, K., Morohoshi, F., Yokoyama, A., Mitsuhashi, N., Shimizu, K. *et al.* (1998). The AML1-MTG8 leukemic fusion protein forms a complex with a novel member of the MTG8(ETO/CDR) family, MTGR1. *Mol. Cell. Biol.* **18**, 846–858.
34. Mulloy, J. C., Cammenga, J., MacKenzie, K. L., Berguido, F. J., Moore, M. A. & Nimer, S. D. (2002). The AML1-ETO fusion protein promotes the expansion of human hematopoietic stem cells. *Blood*, **99**, 15–23.
35. Schessl, C., Rawat, V. P., Cusan, M., Deshpande, A., Kohl, T. M., Rosten, P. M. *et al.* (2005). The AML1-ETO fusion gene and the FLT3 length mutation collaborate in inducing acute leukemia in mice. *J. Clin. Invest.* **115**, 2159–2168.
36. Tomasson, M. H., Sternberg, D. W., Williams, I. R., Carroll, M., Cain, D., Aster, J. C. *et al.* (2000). Fatal myeloproliferation, induced in mice by TEL/PDGFbetaR expression, depends on PDGFbetaR tyrosines 579/581. *J. Clin. Invest.* **105**, 423–432.
37. Carr, D. W., Stofko-Hahn, R. E., Fraser, I. D., Bishop, S. M., Acott, T. S., Brennan, R. G. & Scott, J. D. (1991). Interaction of the regulatory subunit (RII) of cAMP-dependent protein kinase with RII-anchoring proteins occurs through an amphipathic helix binding motif. *J. Biol. Chem.* **266**, 14188–14192.
38. Taylor, S. S., Yang, J., Wu, J., Haste, N. M., Radzio-Andzelm, E. & Anand, G. (2004). PKA: a portrait of protein kinase dynamics. *Biochim. Biophys. Acta*, **1697**, 259–269.
39. Park, S., Speck, N. A. & Bushweller, J. H. (2009). The role of CBFbeta in AML1-ETO's activity. *Blood*, **114**, 2849–2850.
40. Jarnaess, E., Ruppelt, A., Stokka, A. J., Lygren, B., Scott, J. D. & Tasken, K. (2008). Dual specificity A-kinase anchoring proteins (AKAPs) contain an additional binding region that enhances targeting of protein kinase A type I. *J. Biol. Chem.* **283**, 33708–33718.
41. Fiedler, S. E., Schillace, R. V., Daniels, C. J., Andrews, S. F. & Carr, D. W. (2010). Myeloid translocation gene 16b is a dual A-kinase anchoring protein that interacts selectively with plexins in a phospho-regulated manner. *FEBS Lett.* **584**, 873–877.
42. Cozzio, A., Passegue, E., Ayton, P. M., Karsunky, H., Cleary, M. L. & Weissman, I. L. (2003). Similar MLL-associated leukemias arising from self-renewing stem cells and short-lived myeloid progenitors. *Genes Dev.* **17**, 3029–3035.
43. So, C. W., Karsunky, H., Passegue, E., Cozzio, A., Weissman, I. L. & Cleary, M. L. (2003). MLL-GAS7 transforms multipotent hematopoietic progenitors and induces mixed lineage leukemias in mice. *Cancer Cell*, **3**, 161–171.
44. Huntly, B. J., Shigematsu, H., Deguchi, K., Lee, B. H., Mizuno, S., Duclos, N. *et al.* (2004). MOZ-TIF2, but not BCR-ABL, confers properties of leukemic stem cells to committed murine hematopoietic progenitors. *Cancer Cell*, **6**, 587–596.

45. Kwok, C., Zeisig, B. B., Dong, S. & So, C. W. (2006). Forced homo-oligomerization of RARalpha leads to transformation of primary hematopoietic cells. *Cancer Cell*, **9**, 95–108.
46. Terman, J. R. & Kolodkin, A. L. (2004). Nervy links protein kinase A to plexin-mediated semaphorin repulsion. *Science*, **303**, 1204–1207.
47. Gorczynski, M. J., Grembecka, J., Zhou, Y., Kong, Y., Roudaia, L., Douvas, M. G. *et al.* (2007). Allosteric inhibition of the protein–protein interaction between the leukemia-associated proteins Runx1 and CBFbeta. *Chem. Biol.* **14**, 1186–1197.
48. Sheffield, P., Garrard, S. & Derewenda, Z. (1999). Overcoming expression and purification problems of RhoGDI using a family of "parallel" expression vectors. *Protein Expression Purif.* **15**, 34–39.
49. Cierpicki, T. & Bushweller, J. H. (2004). Charged gels as orienting media for measurement of residual dipolar couplings in soluble and integral membrane proteins. *J. Am. Chem. Soc.* **126**, 16259–16266.
50. Yang, D. W., Venters, R. A., Mueller, G. A., Choy, W. Y. & Kay, L. E. (1999). TROSY-based HNCO pulse sequences for the measurement of (HN)-H-1-N-15, N-15-(CO)-C-13, (HN)-H-1-(CO)-C-13, (CO)-C-13-C-13(alpha) and (HN)-H-1-C-13(alpha) dipolar couplings in N-15, C-13, H-2-labeled proteins. *J. Biomol. NMR*, **14**, 333–343.
51. Brunger, A. T., Adams, P. D., Clore, G. M., DeLano, W. L., Gros, P., Grosse-Kunstleve, R. W. *et al.* (1998). Crystallography & NMR system: a new software suite for macromolecular structure determination. *Acta Crystallogr. Sect. D*, **54**, 905–921.
52. Cornilescu, G., Delaglio, F. & Bax, A. (1999). Protein backbone angle restraints from searching a database for chemical shift and sequence homology. *J. Biomol. NMR*, **13**, 289–302.
53. Clore, G. M., Gronenborn, A. M. & Bax, A. (1998). A robust method for determining the magnitude of the fully asymmetric alignment tensor of oriented macromolecules in the absence of structural information. *J. Magn. Reson.* **133**, 216–221.